Food Bioscience 85 (2026) 110224



Contents lists available at ScienceDirect

Food Bioscience

journal homepage: www.elsevier.com/locate/fbio



Online volatilome dynamics of *Lactiplantibacillus plantarum* WCFS1 during growth in MRS, and comparative insights with other wine-associated strains

Antonia Corvino [a,b,*], Emanuela Betta [a], Iuliia Khomenko [a], Vittorio Capozzi [c], Franco Biasioli [a], Mariagiovanna Fragasso [d,**]

[a] Research and Innovation Centre, Fondazione Edmund Mach, via E. Mach 1, San Michele all'Adige, (TN), 38098, Italy
[b] Center for Agriculture Food Environment C3A, University of Trento, San Michele all'Adige, Trento, (TN), Italy
[c] National Research Council of Italy, Institute of Sciences of Food Production (ISPA), c/o CS-DAT, via Michele Protano, Foggia, 71121, Italy
[d] Department of Agriculture, Food, Natural Science, and Engineering (DAFNE), University of Foggia, Foggia, 71122, Italy

ARTICLE INFO

Online volatilome of *L. plantarum* WCFS1

Keywords:
Lactiplantibacillus plantarum
Proton-transfer-reaction time-of-flight mass spectrometry (PTR-ToF-MS)
Gas chromatography
Mass spectrometry (GC-MS)
Volatile organic compounds
Lactic acid bacteria
Fermentation
Microbial metabolomics

ABSTRACT

Lactiplantibacillus plantarum is a metabolically versatile and ecologically adapted lactic acid bacterium widely used in food fermentations. *L. plantarum* WCFS1, originally isolated from human saliva, represents one of the best-characterised model organisms in lactic acid bacteria research. However, knowledge of its volatilome dynamics during bacterial growth in microbiological media remains limited, although these conditions are relevant for studies that combine microbial biology with the evaluation of food-application potential. In the present study, proton-transfer-reaction time-of-flight mass spectrometry (PTR-ToF-MS) was applied to monitor, across eight fermentation cycles, the online evolution of the volatilome of *L. plantarum* WCFS1 grown in MRS medium. To also provide a comparative ecological perspective under standardised conditions, five wine-associated *L. plantarum* strains previously isolated from oenological products were included for comparative analysis. Gas chromatography–mass spectrometry (GC-MS) was employed as a complementary approach to support tentative metabolite annotation. Overall, 142 mass peaks differed significantly from the uninoculated medium, of which 133 were associated with a chemical formula, and 99 were tentatively identified. Multivariate analyses showed that fermentation time was the main source of volatilome variation, with the first four cycles corresponding to the most dynamic metabolic phase and later cycles reflecting stabilisation during stationary growth. Four main kinetic VOC profiles were identified: volatile depletion, transient accumulation, progressive accumulation, and late-stage recovery. Shared metabolites across strains included sulfur compounds, organic acids, branched-chain aldehydes/alcohols, and pyruvate-derived metabolites associated with carbohydrate and amino acid metabolism. WCFS1 showed a distinctive late-stage volatilome, with higher accumulation of pyruvate-, sulfur-, and lipid-related VOCs than wine-associated strains. These results support PTR-ToF-MS as an online sensor for microbial volatilomics and highlight strain-dependent volatile metabolism in *L. plantarum*.

1. Introduction

Lactic acid bacteria are diverse microorganisms that produce lactic acid during carbohydrate metabolism and are common in environments such as plants, the gastrointestinal tract, and fermented foods (Jo et al., 2025; Yang et al., 2024). LAB are recognised for their significant role in biotechnology, as they can produce metabolites of industrial, nutritional, and functional relevance (Cirat et al., 2024). Their metabolic versatility is associated with applications in bio-based solutions, agri-food biotechnology, and probiotic formulations for both animal and human health (Presutto et al., 2026), and for their ability to ferment a broad range of substrates and to improve the microbiological safety, sensory attributes, and nutritional quality of food products (Abedin et al., 2024). Among LAB, species formerly included in the genus *Lactobacillus* (now referred to as lactobacilli and reclassified into different genera) represent one of the most relevant groups in food

* Corresponding author. Research and Innovation Centre, Fondazione Edmund Mach, via E. Mach 1, San Michele all'Adige, 38098, (TN), Italy.
** Corresponding author. Department of Agriculture, Food, Natural Science, and Engineering (DAFNE), University of Foggia, Foggia, 71122, Italy.
E-mail addresses: antonia.corvino@fmach.it (A. Corvino), mariagiovanna.fragasso@unifg.it (M. Fragasso).

https://doi.org/10.1016/j.fbio.2026.110224
Received 2 June 2026; Received in revised form 3 October 2026; Accepted 9 October 2026
Available online 12 October 2026
2212-4292/© 2026 The Authors. Published by Elsevier Ltd. This is an open access article under the CC BY-NC-ND license (http://creativecommons.org/licenses/by-nc-nd/4.0/).

biotechnology (Banicod et al., 2026). Following recent taxonomic reclassification, *Lactiplantibacillus plantarum* has emerged as one of the most extensively investigated species among lactobacilli (and among LAB) due to its remarkable ecological adaptability and technological versatility. *L. plantarum* is capable of colonising a broad range of ecological niches, including the gastrointestinal tract of mammals, human saliva, and numerous fermented food matrices such as sourdough, olives, fermented vegetables, sausages, cheese, and wine (Aljohani et al., 2025; Li et al., 2023). This ecological flexibility is attributed to its robust fermentative metabolism, high acidification capacity, and ability to synthesise antimicrobial metabolites. In fact, including *L. plantarum* in fermentation processes has been associated with improvements in flavour, texture, shelf life, and nutritional quality (Cirat et al., 2024). Furthermore, this species contributes to the functional properties of fermented foods by biosynthesising bioactive compounds, including exopolysaccharides, γ-aminobutyric acid (GABA), riboflavin, and volatile organic compounds (VOCs) (Montagano et al., 2025; Moretton et al., 2025; Qian et al., 2026). Among strains of this species, *L. plantarum* WCFS1 is one of the best-characterised model strains in LAB research, owing to its fully sequenced genome and the extensive characterisation of its physiological, genetic, and metabolic traits. Originally isolated from human saliva, WCFS1 has been widely employed as a reference strain to investigate adaptation mechanisms, probiotic functionality, and metabolic versatility in *L. plantarum* (Kleerebezem et al., 2003; van den Nieuwboer et al., 2016). Despite the extensive genomic and functional knowledge available for this strain, comparatively little information exists about its volatilome during bacterial growth and fermentation (van den Nieuwboer et al., 2016). Because volatile metabolites can reflect microbial physiology and metabolic adaptation, characterising volatilome dynamics in WCFS1 may deepen understanding of this strain as a model for metabolic behaviour and its potential technological implications (Teusink et al., 2006).

The study of microbial VOCs has recently emerged as a promising field of research because these metabolites provide valuable insights into microbial physiology, ecological adaptation, and metabolic activity (Deng et al., 2025). Microorganisms synthesise a wide range of VOCs, including alcohols, aldehydes, ketones, hydrocarbons, aromatic compounds, and sulfur- and nitrogen-containing molecules. The biosynthesis of these compounds is linked to several metabolic pathways, including carbohydrate fermentation, amino acid catabolism, fatty acid metabolism, sulfur metabolism, and terpene biosynthesis (Deng et al., 2025). In fermented food systems, VOCs are particularly relevant because they significantly contribute to flavour development and can serve as metabolic biomarkers for monitoring microbial activity during fermentation (Corvino, Khomenko, et al., 2026). Recent studies have investigated VOCs production by LAB, predominantly using gas chromatography–mass spectrometry (GC-MS)-based approaches, to characterise strain-specific volatile profiles and their contribution to fermentation aroma development (Xing et al., 2025). However, these studies have mainly focused on endpoint characterisation of VOC profiles or comparisons among fermentation conditions, providing limited information on the temporal evolution of volatile metabolites during microbial growth. In this context, direct injection mass spectrometric techniques (DIMS), especially proton-transfer-reaction time-of-flight mass spectrometry (PTR-ToF-MS), offer the possibility to overcome some limitations of conventional chromatographic approaches by enabling rapid, high-throughput, and online monitoring of VOC changes with minimal sample preparation (Corvino et al., 2024; Mazzucotelli et al., 2022). This capability makes PTR-ToF-MS particularly suitable for investigating dynamic microbial responses during growth and fermentation processes. More recently, PTR-ToF-MS has also been applied to monitor VOC production by LAB strains, including *L. plantarum*, enabling the comparison of strain-dependent volatile profiles under different fermentation conditions (Rajendran et al., 2024, 2025). Nevertheless, these studies relied on discrete sampling points during fermentation, whereas high-temporal-resolution online monitoring of VOC evolution throughout microbial growth remains largely unexplored. Furthermore, interpreting PTR-ToF-MS fingerprints often benefits from complementary analytical techniques, such as gas GC-MS, which support compound annotation and improve metabolite identification (Corvino, Khomenko, et al., 2026; Mazzucotelli et al., 2022).

Therefore, the primary aim of the present study was to characterise the volatilome dynamics of *L. plantarum* WCFS1 during growth in MRS medium using PTR-ToF-MS. In addition, to provide a broader ecological perspective on strain-dependent volatile production, we included five additional *L. plantarum* isolates from wine environments as comparative strains. These strains were selected because they originate from a fermentation environment where volatile metabolism is particularly relevant, allowing us to explore whether ecological origin is associated with differences in volatilome profiles. This secondary objective was to assess whether strains originating from different ecological niches exhibited distinct volatilome signatures when cultivated under identical conditions.

2. Materials and methods

2.1. Bacterial strains, sample preparation, and growth monitoring

Six *Lactiplantibacillus plantarum* strains (designated as A, B, C, D, E and F) were included in this study. Five commercially available strains (A, B, C, D, and F) were previously characterised for their protechnological properties in winemaking and were sourced from the Industrial Microbiology Laboratory strain collection at the University of Foggia (Italy). The commercial starter cultures from which the strains were isolated are single-strain cultures tailored to promote malolactic fermentation by reducing the malic acid content to below 0.5 g/l malic acid in wines. Strain E, corresponding to the reference strain *L. plantarum* WCFS1, originally isolated from human saliva, was selected as the primary model strain of the study. Prior to experimentation, all strains were propagated overnight in De Man, Rogosa and Sharpe (MRS) broth (Oxoid, UK) at 30 °C for 24 h. The MRS medium was prepared according to the manufacturer instructions by dissolving 52 g of lyophilised powder in 1 L of distilled water. After pre-cultivation, bacterial suspensions were inoculated at an initial concentration of approximately 10^6 CFU/mL into 3 mL of MRS broth in 20 mL glass vials for VOC measurements. For each strain, six independent biological replicates were prepared. Vials were hermetically sealed with screw caps fitted with silicon/polytetrafluoroethylene (PTFE) septa and incubated under optimal growth conditions (30 °C, pH 6.2) for 32 h. VOC measurements started after 4 h of incubation, considered the minimum equilibration period required to allow sufficient accumulation of microbial volatile compounds in the vial headspace and obtain reliable analytical signals. Volatile measurements were conducted every 4 h (4, 8, 12, 16, 20, 24, 28, and 32 h), yielding eight sampling time points during bacterial growth.

Bacterial growth was monitored in MRS broth for all six *L. plantarum* strains using three independent biological replicates. Optical density at 600 nm (OD600) was recorded every hour for 32 h using a spectrophotometer, after blank correction with sterile MRS medium. The growth curve was fitted using the modified Gompertz model (Zwietering et al., 1990), and growth phases were defined based on the estimated kinetic parameters. The PTR-ToF-MS sampling cycles were compared with the corresponding growth curves to provide a reference framework for the temporal interpretation of the volatilome (Fig. S1).

2.2. Volatile organic compound (VOC) analysis

2.2.1. Proton-transfer-reaction time-of-flight mass spectrometry (PTR-ToF-MS)

VOCs released during bacterial growth were analysed using a commercial PTR-ToF-MS instrument (PTR-TOF 8000; Ionicon Analytik

GmbH, Innsbruck, Austria) operated in standard V-mode configuration. Ionisation conditions in the drift tube were set to a drift temperature of 110 °C, a drift pressure of 2.30 mbar, and a drift voltage of 550 V, yielding an E/N ratio of approximately 140 Townsend (1 Td = 10^{-17} V cm^2), where E represents the electric field strength and N the gas number density. Sample introduction was achieved via a heated polyether ether ketone (PEEK) capillary tube (internal diameter: 0.04 inches) maintained at 110 °C, with an inlet flow rate of 40 sccm. Mass spectra were acquired at a rate of one spectrum per second. VOC measurements were performed automatically using a multipurpose autosampler (Gerstel GmbH, Mülheim an der Ruhr, Germany), following procedures previously described by Makhoul et al. (Makhoul et al., 2014). Each sample was analysed every 4 h, a time interval established in preliminary experiments as sufficient to allow VOC accumulation in the vial headspace. To minimise microbiological and chemical contamination between analyses, a gas calibration unit (GCU; Ionicon Analytik GmbH, Innsbruck, Austria) was employed to generate zero air for flushing the sampling line and inlet system, and for use between measurements (Rajendran et al., 2024). PTR-MS technology enables rapid VOC detection, with limits of detection down to parts-per-trillion-by-volume (pptv). Coupling PTR with time-of-flight mass analysers further improves temporal and mass resolution, enabling online monitoring of volatilome dynamics during microbial fermentation processes. The automated analytical workflow used in this study followed approaches previously reported in food fermentation applications.

2.2.1.1. PTR-ToF-MS spectral data processing. Dead-time correction, internal mass calibration, and peak extraction were performed using procedures previously described by Cappellin et al. (2011) with a modified Gaussian peak-shape model. Peak intensities were estimated in parts per billion by volume (ppbv) using established literature methods, assuming a constant reaction rate coefficient (k = 2×10^{-9} cm^3 s^{-1}). Although this assumption may introduce systematic uncertainty in the absolute concentrations of individual compounds, associated errors are generally below 30% and can be corrected when compound-specific reaction coefficients are available.

An initial dataset of 142 ion masses was obtained after peak extraction. To remove background signals originating from the analytical system and sample vials, ion masses were compared with blank measurements (empty sealed vials routinely analysed between consecutive samples) using one-way ANOVA ($p < 0.05$). Ion masses that were not significantly different from the blanks were considered background signals and excluded from further analyses. No multiple-testing correction was applied, as this analysis served exclusively as a preliminary quality-control filtering step to remove background signals before downstream statistical analyses. Subsequently, water clusters and isotopic peaks were removed, resulting in a dataset of 133 ion masses. Putative elemental formulas were assigned to the remaining ion masses using the "Elemental Composition Calculator" and "Molecular Weight Calculator" integrated into the PTR-ToF-MS software, yielding 113 ion masses with assigned elemental formulas. Tentative compound annotation was subsequently achieved by integrating accurate mass information with GC-MS data obtained from the reference strain *L. plantarum* WCFS1, the PTR-ToF-MS compound assignment guide (Yáñez-Serrano et al., 2021), and previously reported VOCs associated with lactic acid bacteria (Rajendran et al., 2024, 2025). Using this approach, 99 ion masses were tentatively assigned to specific volatile compounds. All PTR-ToF-MS spectral data were processed and analysed using MATLAB R2017a (MathWorks Inc., Natick, MA, USA) and R software (version 4.4.0; R Foundation for Statistical Computing, Vienna, Austria).

2.2.2. Gas chromatography–mass spectrometry (GC-MS)

GC-MS analyses were performed exclusively on the reference strain WCFS1 (strain E), which represented the primary model strain of this study, to support VOC annotation and interpretation of PTR-ToF-MS signals. Uninoculated MRS medium was analysed as a control to aid compound discrimination and VOC identification. Samples were collected throughout the entire fermentation process (0–32 h), resulting in nine sampling time points (0, 4, 8, 12, 16, 20, 24, 28, and 32 h). Unlike PTR-ToF-MS, which started after 4 h to allow sufficient accumulation of VOCs in the vial headspace for reliable online measurements, GC-MS also included the initial 0 h sample to provide a complete temporal reference for metabolite annotation. At each sampling time, two independent biological replicates of inoculated MRS broth and two independent biological replicates of uninoculated MRS medium were analysed. Because PTR-ToF-MS was the primary analytical platform for continuous volatilome monitoring, and GC-MS was used as a complementary technique to support VOC annotation, GC-MS data were not used for inferential statistical analysis of volatilome dynamics. VOCs were extracted by headspace solid-phase microextraction (HS-SPME) using a 2 cm fibre coated with divinylbenzene/carboxen/polydimethylsiloxane (DVB/CAR/PDMS; 50/30 μm; Supelco, Bellefonte, PA, USA). The SPME fibre was exposed to the vial headspace for 40 min at the same incubation temperature used for bacterial cultivation. Adsorbed compounds were thermally desorbed in the GC injector port at 250 °C for 5 min. GC-MS analysis was carried out using a Clarus 500 GC-MS system (PerkinElmer, Norwalk, CT, USA) equipped with an electron ionisation (EI) source operating at 70 eV and a scan range of m/z 33–350. Chromatographic separation was achieved using an HP-INNOWax fused-silica capillary column (30 m × 0.32 mm internal diameter × 0.5 μm film thickness; Agilent Technologies, Palo Alto, CA, USA). Helium was used as the carrier gas at a constant flow rate of 2.0 mL/min. The oven temperature programme was as follows: an initial temperature of 40 °C for 1 min, increased at 5 °C min^{-1} to 250 °C, followed by a 2 min final hold. Compound identification was performed by comparing mass spectra with the NIST14 and Wiley 7th Mass Spectral Libraries and by comparing experimentally determined linear retention indices (LRI) with literature values. LRIs were calculated under identical chromatographic conditions following injection of a C7–C30 n-alkane standard mixture (Supelco).

2.3. Statistical analysis

Statistical analyses were performed using PTR-ToF-MS data (133 retained mass peaks) obtained from six independent biological replicates for each *L. plantarum* strain. Each biological replicate was treated as an independent observation in all statistical analyses, and no averaging across replicates was performed. No biological replicates were excluded from the dataset, and no missing values were present; therefore, no imputation procedures were required. Multivariate statistical analyses, including principal component analysis (PCA) and partial least squares discriminant analysis (PLS-DA), were applied to log-transformed and autoscaled (unit-variance scaling) datasets to evaluate differences in VOC emission profiles among *L. plantarum* strains during growth in MRS broth. The optimal number of PLS-DA components was determined by 5-fold cross-validation repeated 50 times, evaluating the Balanced Error Rate (BER) using centroid distance. Five components were retained, accounting for 80.6% of the X variance and yielding a BER of 0.35. Discriminant variables were identified based on the Variable Importance in Projection (VIP) score, selecting ion masses with VIP > 1.0. Additionally, compounds with VIP < 1.0 were retained when they showed distinctive strain-specific emission patterns or were confirmed by GC-MS analysis, due to their biological relevance. Data visualisation and statistical analyses were performed using custom R (v. 4.4.0; R Core Team, 2024) scripts and the external packages mixOmics and ggplot2.

3. Results

3.1. Global volatilome evolution during fermentation

PTR-ToF-MS was used to monitor the online evolution of the volatilome of *L. plantarum* strains during growth in MRS medium under optimal cultivation conditions. The experimental set included the reference strain *L. plantarum* WCFS1 (hereafter, strain E) and five wine-associated strains (A, B, C, D, and F) selected for their pro-technological potential in oenology. Following the data-processing workflow described in Section 2.2.1.1, 113 ion masses with assigned elemental formulas were retained for downstream analyses, of which 99 were tentatively annotated at the compound level. To obtain an overview of the volatilome evolution during bacterial growth, principal component analysis (PCA) was performed on the processed PTR-ToF-MS dataset, including both inoculated samples and uninoculated MRS medium as a control. The PCA score plot showed good experimental repeatability, as biological replicates of each sample followed comparable trajectories across the eight fermentation cycles (Fig. 1). The first two principal components explained 87.66% of the total variance, with PC1 accounting for 71.34% and PC2 for 16.32%. The distribution of samples along PC1 revealed a marked time-dependent evolution of the volatilome. PCA highlighted a common temporal trajectory across fermentation cycles, along with strain-dependent differences within this overall pattern. Strains B and D followed highly similar volatilome profiles, while strains A and F showed comparable trajectories. Strain C exhibited a profile close to those of strains B and D during the first four cycles, followed by partial divergence in later fermentation stages. By contrast, strain E (WCFS1) showed the most distinctive trajectory, separating from the wine-associated strains, particularly during the late growth phases (i.e., late stationary phase) (Fig. 2). These results indicate that *L. plantarum* growth is a relevant driver of volatilome variation. In contrast, strain identity contributed additional differentiation, particularly for WCFS1. To further investigate VOCs associated with the fermentation stage, partial least squares discriminant analysis (PLS-DA) was performed, with the fermentation cycle as the classification variable (Fig. 2A). The PLS-DA score plot confirmed the temporal organisation observed in the PCA. Along PLS-DA Component 1, samples were progressively distributed by fermentation cycle, with cycle 1 corresponding to the first 4 h of fermentation and representing the earliest sampling stage (Fig. 2A). This cycle was clearly separated from the subsequent cycles. Fig. S2 reports the growth profile of all strains in detail. This initial separation may reflect the specific volatilome profile accumulated during the transition into active growth, considering that PTR-ToF-MS cycles integrate VOC emission over a 4 h sampling period rather than representing instantaneous measurements. Cycle 2 and3 represented intermediate stagesof fermentation, while cycles 4 to 8 (16–32 h), corresponded to the later stages of fermentation and showed greater overlap, indicating a more stable but still evolving volatilome during the late fermentation period. PLS-DA Component 2 further contributed to the separation between early, intermediate, and late fermentation stages. In particular, intermediate fermentation cycles were distinguished from those in both the initial and late-stage samples. The PLS-DA loading plot identified the mass peaks that contributed most strongly to the separation among fermentation cycles (Fig. 2B), providing the basis for selecting the dominant VOCs reported in Table 1.

3.2. Temporal evolution of VOC profiles during fermentation

Table 1 reports the relevant mass peaks selected for their contributions across fermentation cycles, including the protonated formula, tentative identification where available, and the observed temporal trend. The temporal evolution of VOCs was heterogeneous across the dataset. To support biological interpretation, ions with well-defined temporal behaviours were visually grouped into four descriptive kinetic profiles based on the overall shape of their temporal trajectories

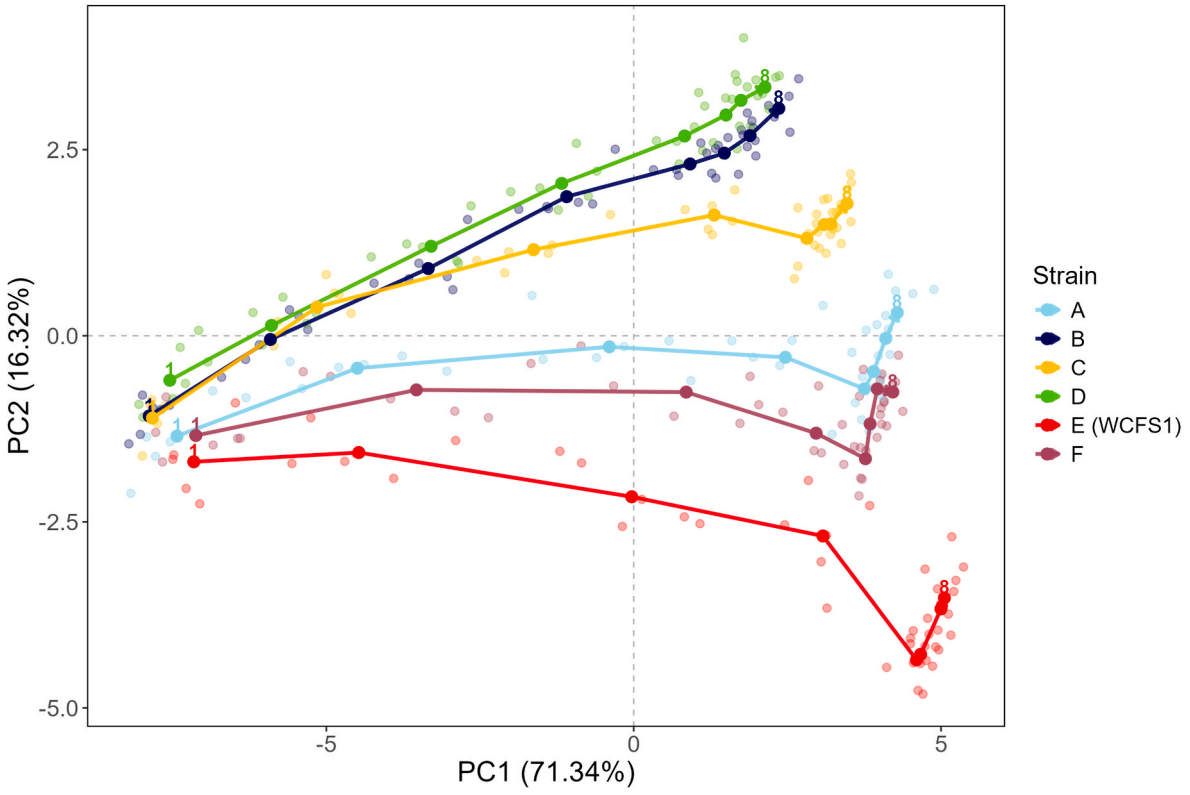


Fig. 1. Principal component analysis (PCA) score plot of PTR-ToF-MS volatilome profiles from *Lactiplantibacillus plantarum* strains grown in MRS medium. Samples are coloured according to strain. Point size indicates fermentation cycle from 1 to 8. Lines connect consecutive fermentation cycles within each strain to illustrate the temporal evolution of volatilome profiles during growth.

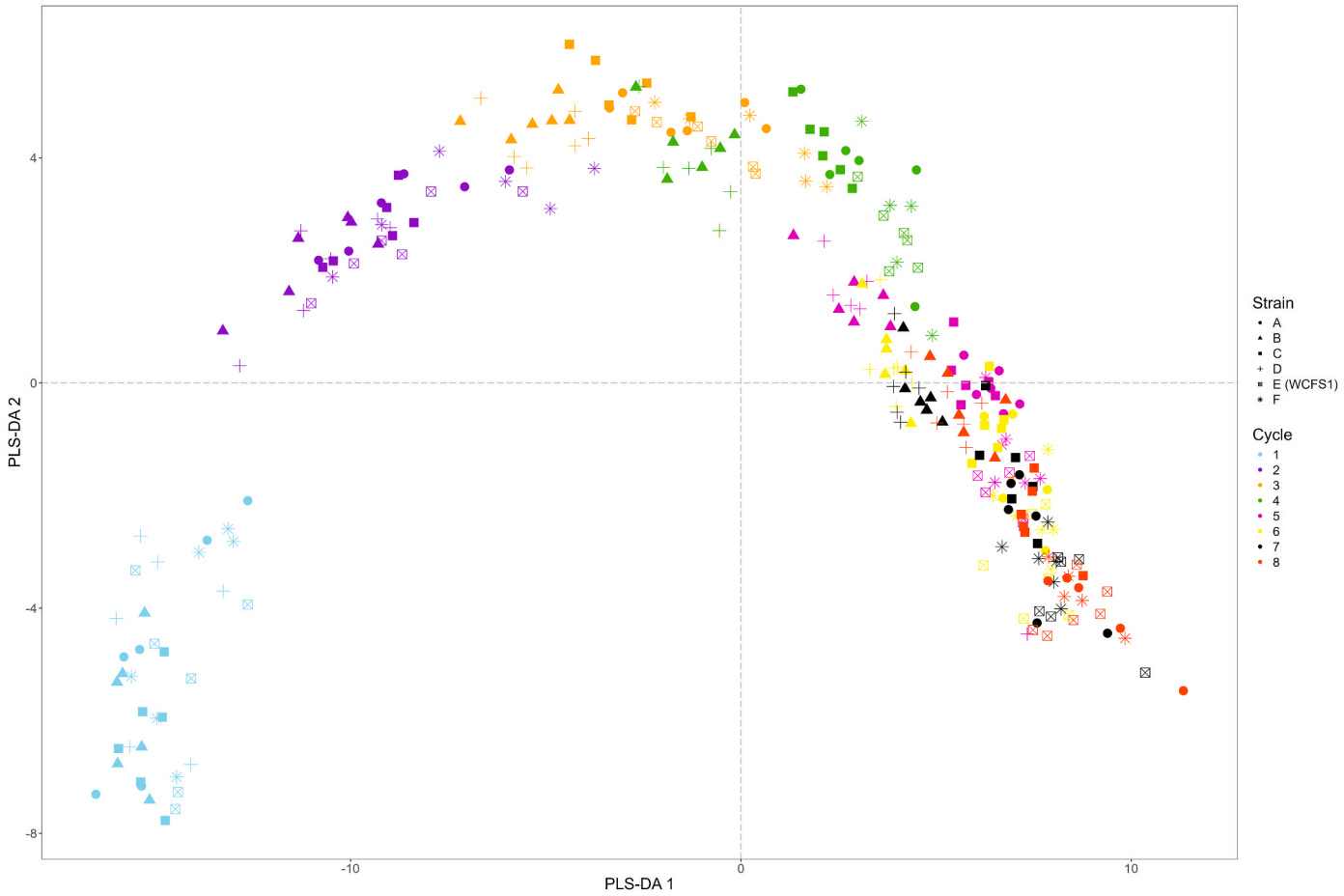


Fig. 2A. Partial least squares discriminant analysis (PLS-DA) score plot of PTR-ToF-MS volatilome profiles from *Lactiplantibacillus plantarum* strains grown in MRS medium. Colours represent the eight fermentation cycles (Cycles 1–8), which were used as the response classes in the supervised PLS-DA model, whereas symbols identify the six *L. plantarum* strains.

across the eight fermentation cycles. Profile A (transient accumulation), Profile B (progressive accumulation), Profile C (depletion), and Profile D (late-stage recovery) comprised 11, 30, 20, and 6 ions, respectively, whereas ions showing flat or irregular trajectories were not assigned to any profile. The temporal profiles were consistent across the six *L. plantarum* strains, although signal intensity differed, particularly for the reference strain E (WCFS1), while the overall temporal patterns remained conserved. Fig. 3 shows representative examples. The first profile, hereafter referred to as profile A, increased progressively up to approximately cycle 5, then decreased during late fermentation. This trend was represented by m/z 49.010, assigned to the protonated formula (p.f.) CH_4SH^+ and tentatively identified (t.i.) as methanethiol (Fig. 3). Methanethiol showed a marked increase during the central phase of fermentation, with the highest values generally observed around cycle 5, followed by a decline towards cycles 7 and 8. This profile was observed in several strains, although with different intensities; strains A, E, and F showed the highest accumulation, whereas the uninoculated medium remained low during the early and intermediate cycles and increased only at later time points. The second profile, profile B, showed a progressive increase during the first fermentation cycles, followed by stabilisation or a slower rise toward the end of the experiment. This behaviour was represented by m/z 61.028 t.i. as acetic acid (p.f. $C_2H_4O_2H^+$), which showed a continuous increase across all inoculated samples, with strain E among the highest emitters in the late cycles (Fig. 3). Similar profile B trends were observed for several compounds associated with later fermentation stages, including signals listed in Table 1 and in the supplementary kinetic plots. Profile C (the third profile) was defined by progressive depletion during fermentation. The representative ion at m/z 107.051 was t.i.as benzaldehyde (p.f. $C_7H_6OH^+$) (Fig. 3). This compound showed a high initial abundance, followed by a marked decrease across all inoculated samples. The decline was faster and more pronounced in inoculated samples than in the uninoculated medium, suggesting that bacterial growth strongly affected this signal. Other VOCs with profile C were mainly associated with the early fermentation stage and included m/z 145.122, t.i.as octanoic acid (p.f. $C_8H_{16}O_2H^+$); m/z 73.065, t.i.as 2-butanone (p.f. $C_4H_8OH^+$); m/z 75.070, t.i.as 1-butanol (p.f. $C_4H_{10}OH^+$); m/z 87.080, t.i.as 2-methylbutanal/3-methylbutanal (p.f. $C_5H_{10}OH^+$); and m/z 89.087, t.i.as 3-methyl-1-butanol (p.f. $C_5H_{12}OH^+$). Profile D showed an initial decrease, followed by a plateau and, in some strains, a subsequent increase during the late fermentation phase. This trend was represented by m/z 83.085, assigned to p.f $C_6H_{11}^+$ and tentatively reported as unknown (Fig. 3). This ion showed a rapid decrease from cycle 1 to cycle 2 or 3 in most strains, followed by strain-dependent behaviour during later cycles. Notably, strain E displayed a secondary increase around cycles 5–6, whereas most other strains remained comparatively lower. Several ions contributed specifically to discriminating between individual fermentation cycles, as indicated by the PLS-DA loading plot (Fig. 3B) and summarised in Table 1. Cycle 1 was mainly associated with VOCs exhibiting profile C, including m/z values of 107.051, 145.122, 73.065, 75.070, 87.080, and 89.087. These signals were abundant at the start of incubation and decreased progressively during bacterial growth. The mass peak at m/z 147.098 t.i. as pentanoic acid, 2-hydroxy-4-methyl-, methyl ester (p.f. $C_7H_{14}O_3H^+$), showed a different pattern in strain E: it decreased similarly to the other strains until cycle 4, then increased again in the following cycles. A limited number of discriminant VOCs

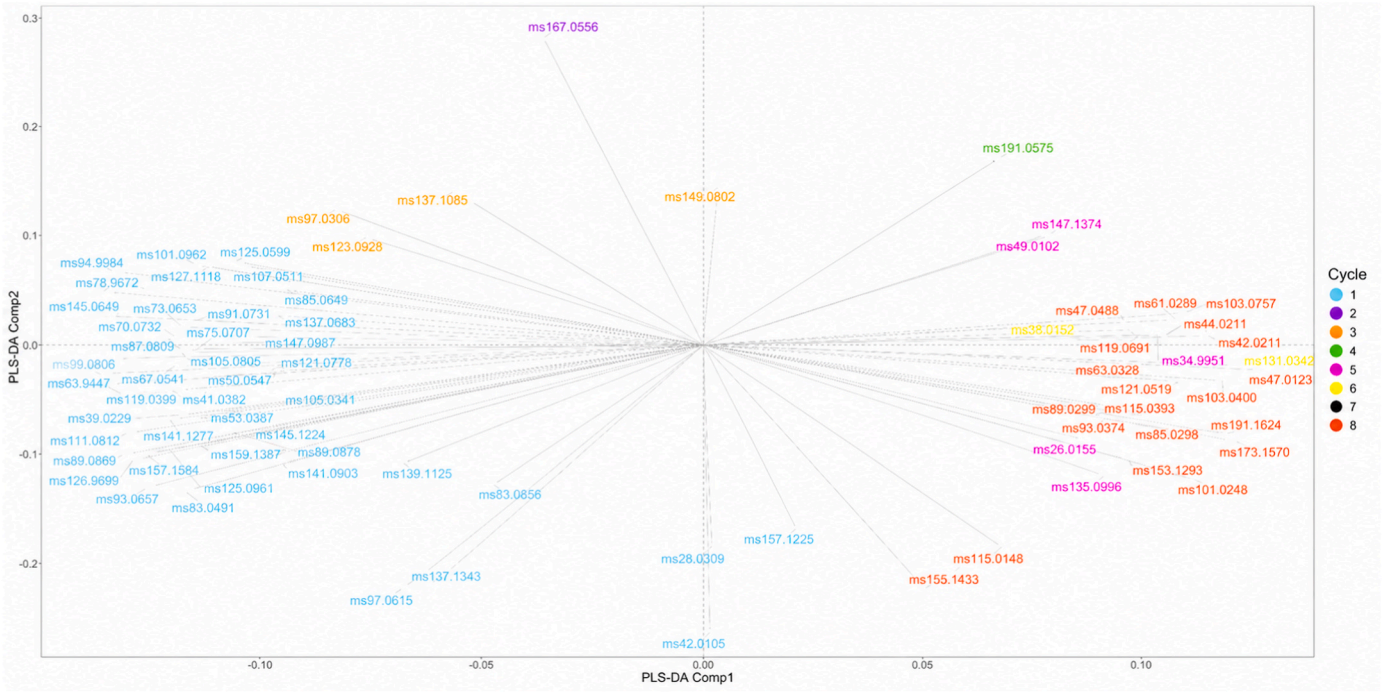


Fig. 2B. PLS-DA loading plot showing PTR-ToF-MS ions contributing to the discrimination of fermentation cycles in *Lactiplantibacillus plantarum* strains grown in MRS medium. Only mass peaks with Variable Importance in Projection (VIP) > 1 on either Component 1 or Component 2 are labelled (78 out of 133 detected peaks), reflecting their relevance to the discriminant model. Colours correspond to the fermentation cycle with which each ion was mainly associated (i.e., the cycle showing the highest mean intensity).

characterised cycle 2, such as the ion m/z 115.077, t.i. as 2,5-hexanedione (p.f. $C_6H_{10}O_2H^+$), displayed a strain-dependent trend, with strains B and D increasing until cycle 3 before declining. Cycle 3 was associated with VOCs showing profile B, including m/z 113.096, t.i. as 2-heptenal (p.f. $C_7H_{12}OH^+$), and m/z 131.106, t.i. as isoamyl acetate (p.f. $C_7H_{14}O_2H^+$). At the same stage, strain-specific signals also emerged, including m/z 149.080, t.i. as mevalonic acid (p.f. $C_6H_{12}O_4H^+$), and m/z 87.046, t.i. as 2,3-butanedione/diacetyl (p.f. $C_4H_6O_2H^+$), both showing higher values in strain E. Cycle 4 was associated with m/z 169.159, t.i. as 10-undecenal (p.f. $C_{11}H_{20}OH^+$), which showed a profile A-type trend in strains E, F, and A. Cycle 5 included several mass peaks with different kinetic profiles. Among these, m/z 49.010, t. i. as methanethiol, and m/z 67.020, t.i. as furan fragment (p.f. $C_4H_2OH^+$), were particularly evident in strain A. In strain E, m/z 91.024, t.i. as methylthioacetate (p.f. $C_3H_6OSH^+$) and m/z 171.176, t.i. as 2-undecanone (p.f. $C_{11}H_{22}OH^+$) showed a distinctive behaviour. Similarly, m/z 129.127, t. i. as 1-octen-3-ol (p.f. $C_8H_{16}OH^+$) exhibited a characteristic profile in strain F.

Cycles 6 and 7 were mainly characterised by ions with profile B or late-accumulation patterns. At cycle 6, m/z 111.117, tentatively assigned to an acyclic diene or cycloalkene (p.f. $C_8H_{14}H^+$), increased in several strains, whereas the uninoculated medium and strain D showed flatter trends. Conversely, m/z 143.144, t.i. as 2-nonanone (p.f. C9H18OH+), increased only in strains A, E, and F. Other ions showed a clear strain-dependent evolution, with strain E generally reaching the highest values and strains F and A following similar but lower-intensity trends. These included m/z 125.132, tentatively assigned to a diene or cycloalkene group (p.f. $C_9H_{16}H^+$); m/z 161.150, t.i. as 1,9-nonanediol (p.f. $C_9H_{20}O_2H^+$) and m/z 97.101, tentatively assigned to an alkyl fragment (p.f. $C_7H_{12}H^+$). Cycle 7 showed a similar pattern, with m/z 115.112, t.i. as 2-heptanone (p.f. $C_7H_{14}OH^+$), displaying strain-dependent late-stage accumulation. Cycle 8 maintained the late-stage profile observed during cycles 6 and 7. Several mass peaks reached their highest or near-highest values in strain E, including m/z 89.059, t. i. as acetoin/isobutyric acid/butanoic acid (p.f. $C_4H_8O_2H^+$); m/z 71.048, t.i. as 2-butenal (p.f. $C_4H_6OH^+$); and m/z 131.071, t.i. as ethyl acetoacetate (p.f. $C_6H_{10}O_3H^+$). A distinct group of pyrazine-related signals was also detected, including m/z 109.076 (p.f. $C_6H_8N_2H^+$), m/z 123.092 (p.f. $C_7H_{10}N_2H^+$), m/z 137.108 (p.f. $C_8H_{12}N_2H^+$), and m/z 95.060 (p.f $C_5H_6N_2H^+$), mainly associated with cycle 3, and m/z 81.044 (p.f. $C_4H_4N_2H^+$), associated with cycle 8. These compounds showed relatively flat trends across inoculated samples. An exception was m/z 121.077 (p.f. $C_7H_8N_2H^+$), associated with cycle 1, which showed a slight decrease in *L. plantarum* strains; in the uninoculated medium, it initially increased and then decreased. Because these signals were also present in the medium control, their interpretation requires caution.

3.3. Strain-dependent volatilome with emphasis on L. plantarum WCFS1

The PCA score plot indicated that strain E, corresponding to *L. plantarum* WCFS1 (*Lp* WCFS1), exhibited the most distinct volatilome trajectory compared with the five wine-associated strains (Fig. 1). This separation became particularly evident during the late fermentation cycles, suggesting that the *Lp* WCFS1 volatilome diverged mainly during the later stages of fermentation.

The strain-dependent behaviour of *Lp* WCFS1 was further examined through selected VOC trajectories reported in Fig. S3 and the complete kinetic dataset. Twelve mass peaks were particularly informative for describing the distinctive profile of strain E: m/z 63.009 (p.f. $CO_2H_3O^+$, tentatively assigned to carbon dioxide-related signal), m/z 71.048 (p.f. $C_4H_6OH^+$, t.i.as 2-butenal), m/z 87.046 (p.f. $C_4H_6O_2H^+$, t.i.as 2,3-butanedione/diacetyl), m/z 89.059 (p.f. $C_4H_8O_2H^+$, t. i. as acetoin/isobutyric acid/butanoic acid), m/z 91.024 (p.f. $C_3H_6OSH^+$, t.i.as methylthioacetate), m/z 107.097 (unknown), m/z 131.071 (p.f. $C_6H_{10}O_3H^+$, t.i.as ethyl acetoacetate), m/z 143.144 (p.f $C_9H_{18}OH^+$, t.i. as 2-nonanone), m/z 151.142 (p.f $C_{11}H_{18}H^+$, unknown), m/z 169.159 (p.f $C_{11}H_{20}OH^+$, t.i.as 10-undecenal), m/z 171.176 (p.f. $C_{11}H_{22}OH^+$, t.i. as 2-undecanone), and m/z 189.181 (p.f. $C_{11}H_{24}O_2H^+$, t.i.as 1,11-undecanediol). Among these ions, m/z 63.009, m/z 151.142, m/z 169.159 and m/z 171.176 reached their highest values around cycle 5 in strain E, whereas several others increased progressively until the final

Table 1
Dominant volatile organic compounds discriminating fermentation cycles in *Lactiplantibacillus plantarum* strains grown in MRS medium. For each selected PTR-ToF-MS ion, the dominant cycle, measured and theoretical masses, protonated formula, tentative compound identification, VIP scores for the first two PLS-DA components, and strain specificity are reported. Annotation confidence is indicated as follows: compounds marked with an asterisk (*) were supported by HS-SPME-GC-MS analysis performed on the reference strain *L. plantarum* WCFS1; all other compound annotations are tentative and based on PTR-ToF-MS exact mass, molecular formula, and literature evidence; entries described as "fragment" correspond to fragment ions and are not interpreted as unique compound identifications. Because GC-MS analysis was performed only for the reference strain WCFS1, these annotations should not be interpreted as confirmed identifications for the remaining strains. n.i., not identified.

Dominant cycle	Measured mass	Theoretical mass	Protonated formula	Tentative identification	VIP_comp1	VIP_comp2	Strain specificity	Ref.
1	39.022	39.0229	C3H2H+	isoprene fragment	1.368	1.104	common	Yáñez-Serrano et al. (2021)
1	41.038	41.0385	C3H4H+	2-methyl-butyric acid fragment	1.376	1.039	common	(Rajendran et al., 2025; Yáñez-Serrano et al., 2021)
1	42.010	42.0105	C2HO*H+	acetyl fragment	0.005	2.248	common	Rajendran et al. (2025)
1	45.034	45.034	C2H4OH+	acetaldehyde	0.608	0.744	Lp A and F	Rajendran et al. (2024)
1	53.038	53.0385	C4H4H+	cyclobutadiene, butenyne	1.332	1.097	Lp E	Yáñez-Serrano et al. (2021)
1	55.054	55.0542	C4H6H+	1,3-butadiene	1.32	0.974	common	Yáñez-Serrano et al. (2021)
1	63.009	63.0076	CO2*H3O+	carbon dioxide	0.654	0.549	Lp E	(Rajendran et al., 2024, 2025)
1	67.054	67.0542	C5H6H+	3-penten-1-yne, 1,3-cyclopentadiene, monoterpene fragments	1.403	1.021	common	Yáñez-Serrano et al. (2021)
1	73.065	73.0653	C4H8OH+	2-butanone*	1.269	0.935	common	Yáñez-Serrano et al. (2021)
1	75.070	75.0715	C4H10OH+	1-butanol*	1.343	0.967	common	Yáñez-Serrano et al. (2021)
1	78.967	78.967	CH2S2H+	n.i.	1.59	1.24	common	Rajendran et al. (2025)
1	80.986	80.9869	CH4S2H+	methanedithiol	1.549	1.385	common	Yáñez-Serrano et al. (2021)
1	83.049	83.0491	C5H6OH+	3-methylfuran, 2-methylfuran, cyclopentanone, hexenal fragment, hexanol fragment	1.377	1.472	common	Yáñez-Serrano et al. (2021)
1	83.085	83.0855	C6H10H+	cyclic and acyclic unsaturated hydrocarbons	0.576	1.131	Lp E, F and A	Yáñez-Serrano et al. (2021)
1	85.064	85.0647	C5H8OH+	2-ethylacrolein*	0.798	0.693	common	
1	87.080	87.0809	C5H10OH+	2-methyl butanal*, 3-methyl butanal*	1.379	0.994	common	Yáñez-Serrano et al. (2021)
1	89.087	89.0871	C5H12OH+	3-methyl-1-butanol*	1.212	1.115	common	Yáñez-Serrano et al. (2021)
1	91.073	91.0753	C4H10O2H+	2,3-butanediol	1.306	0.965	common	(Rajendran et al., 2024, 2025)
1	93.065	93.0698	C7H8H+	toluene	1.48	1.514	common	Yáñez-Serrano et al. (2021)
1	94.998	94.9983	C2H6S2H+	dimethyl disulfide	1.556	1.287	common	Rajendran et al. (2024)
1	97.061	97.0647	C6H8OH+	2,5-dimethylfuran, cyclohexen-2-one	0.805	1.929	common	(Rajendran et al., 2024, 2025)
1	99.080	99.0804	C6H10OH+	aldehyde, ketone	1.557	1.123	common	Yáñez-Serrano et al. (2021)
1	101.096	101.096	C6H12OH+	hexanal	1.245	1.103	common	Yáñez-Serrano et al. (2021)
1	105.089	105.0915	C5H12O2H+	2-methyl-1,3-butanediol	1.386	0.999	common	
1	107.051	107.0491	C7H6OH+	benzaldehyde*	1.19	1.06	common	Yáñez-Serrano et al. (2021)
1	111.081	111.0804	C7H10OH+	2,3-dimethyl-2-cyclopentenone	1.53	1.277	common	
1	119.039	119.0402	C4H6O4H+	butanedioic acid	1.591	1.177	common	
1	121.077	121.0765	C7H8N2H+	2-ethenyl- 6-methyl-pyrazine*	1.125	0.828	common	
1	125.059	125.0602	C7H8O2H+	guiacol, 2,6-dimethyl-4H-pyran-4-one	1.2	1.077	common	Yáñez-Serrano et al. (2021)
1	125.096	125.096	C8H12OH+	3,5-octadien-2-one	1.418	1.288	common	
1	126.969	126.9676	C5H2S2H+	dimethyltrisulfide	1.52	1.401	common	Yáñez-Serrano et al. (2021)
1	127.111	127.1117	C8H14OH+	1-octen-3-one, 2-octenal	1.21	1.06	common	Yáñez-Serrano et al. (2021)
1	137.068	137.0709	C7H8N2OH+	2-acetyl-3-methylpyrazine	1.044	0.794	common	
1	137.134	137.1324	C10H16H+	monoterpene	0.726	1.898	common	Yáñez-Serrano et al. (2021)
1	139.112	139.1117	C9H14OH+	2-pentylfuran	0.797	1.053	common	Yáñez-Serrano et al. (2021)
1	141.090	141.0915	C8H12O2H+	unsaturated ester, acid	1.112	1.19	common	Yáñez-Serrano et al. (2021)
1	141.127	141.1273	C9H16OH+	2-nonenal, 3-nonen-2-one	1.405	1.136	common	Yáñez-Serrano et al. (2021)
1	145.064	145.0647	C10H8OH+	3-phenylfuran*	1.581	1.173	common	Yáñez-Serrano et al. (2021)

(*continued on next page*)

Table 1 (*continued*)

Dominant cycle	Measured mass	Theoretical mass	Protonated formula	Tentative identification	VIP_comp1	VIP_comp2	Strain specificity	Ref.
1	145.122	145.1228	C8H16O2H+	octanoic acid* (caprylic acid)	1.25	1.118	common	(Rajendran et al., 2024, 2025)
1	147.098	147.1015	C7H14O3H+	pentanoic acid, 2-hydroxy-4-methyl-, methyl ester*	1.218	0.878	Lp E	
1	157.158	157.1586	C10H20H+	decanal, decanone, menthol	1.476	1.342	common	Yáñez-Serrano et al. (2021)
1	159.138	159.1379	C9H18O2H+	ester, nonanoic acid	1.338	1.209	common	Yáñez-Serrano et al. (2021)
2	97.030	97.0284	C5H4O2H+	furfural*	0.901	1.183	common	
2	115.077	115.0753	C6H10O2H+	2,5-hexanedione	0.992	0.945	Lp B and D	Yáñez-Serrano et al. (2021)
3	87.046	87.0466	C4H6O2H+	2,3 butanedione* (diacetyl)	0.011	0.349	Lp E	Yáñez-Serrano et al. (2021)
3	95.060	95.0603	C5H6N2H+	methyl-pyrazine*	0.016	0.375	common	
3	109.076	109.0765	C6H8N2H+	2,5-dimethyl-pyrazine*, 2,6-dimethyl-pyrazine*, 2-cyanomethylene-pyrrolidine*	0.266	0.458	common	Yáñez-Serrano et al. (2021)
3	113.096	113.096	C7H12OH+	2-heptenal	0.295	0.631	common	Yáñez-Serrano et al. (2021)
3	123.092	123.0916	C7H10N2H+	trimethyl-pyrazine*, 2-ethyl, 6-methyl-pyrazine*, 2-ethyl, 5-methyl-pyrazine*	0.611	0.741	common	Yáñez-Serrano et al. (2021)
3	131.106	131.1066	C7H14O2H+	isoamyl acetate	0.182	0.576	common	Rajendran et al. (2024)
3	137.108	137.1073	C8H12N2H+	3-ethyl, 2,5-dimethyl-pyrazine*	0.573	1.105	common	
3	149.080	149.0808	C6H12O4H+	mevalonic acid	0.038	1.212	Lp E	
4	169.159	169.1586	C11H20OH+	10-undecenal	0.544	0.602	Lp E, Lp F, A	
4	191.057	191.0576	C10H9NO3H+	n.i.	0.796	1.58	common	
5	34.995	34.9949	H2SH+	hydrogen sulfide	1.198	0.865	Lp A	Rajendran et al. (2024)
5	49.010	49.0106	CH4SH+	methanethiol	0.875	1.058	Lp A, Lp F, Lp E	Rajendran et al. (2024)
5	67.020	67.0178	C4H2OH+	furan fragment	0.78	1.037	common	
5	91.024	91.0212	C3H6OSH+	methylthioacetate	0.379	0.331	Lp E	Yáñez-Serrano et al. (2021)
5	101.024	101.0233	C4H4O3H+	succinic anhydride	1.314	1.427	common	Yáñez-Serrano et al. (2021)
5	117.090	117.0915	C6H12O2H+	hexanoic acid*	0.199	0.455	common	Rajendran et al. (2024)
5	123.047	123.0446	C7H6O2H+	benzoic acid	0.386	0.665	common	Rajendran et al. (2024)
5	129.127	129.1273	C8H16OH+	1-octen-3-ol	0.178	0.195	Lp F	Yáñez-Serrano et al. (2021)
5	135.099	135.1015	C6H14O3H+	n.i.	1.029	1.231	common	Rajendran et al. (2025)
5	143.036	143.0338	C6H6O4H+	hydroxymaltol	0.868	1.007	common	Yáñez-Serrano et al. (2021)
5	147.137	147.1379	C8H18O2H+	1,8-octanediol	0.923	1.068	common	Yáñez-Serrano et al. (2021)
5	151.142	151.1432	C11H18H+	n.i.	0.45	0.326	Lp E	
5	171.176	171.1743	C11H22OH+	2-undecanone*	0.948	0.712	Lp E, Lp F, Lp A	Yáñez-Serrano et al. (2021)
5	189.181	189.1854	C11H24O2H+	1,11-undecanediol	0.662	0.539	Lp E	Yáñez-Serrano et al. (2021)
6	97.101	97.1011	C7H12H+	alkyl fragment	0.063	0.53	Lp E, Lp F, A	Yáñez-Serrano et al. (2021)
6	111.117	111.1168	C8H14H+	acyclic diene or cycloalkene	0.902	0.652	Lp F	Yáñez-Serrano et al. (2021)
6	125.132	125.1324	C9H16H+	diene or cycloalkene	0.746	0.902	Lp E	Yáñez-Serrano et al. (2021)
6	131.034	131.0338	C5H6O4H+	methylene butanedioic acid	1.431	1.049	common	Yáñez-Serrano et al. (2021)
6	143.144	143.1435	C9H18OH+	2-nonanone*	0.679	0.647	Lp E, Lp F, Lp A	Yáñez-Serrano et al. (2021)
6	161.150	161.1541	C9H20O2H+	1,9-nonanediol	0.645	0.618	Lp E, Lp F, Lp A	Yáñez-Serrano et al. (2021)
7	115.112	115.1117	C7H14OH+	2-heptanone*	0.518	0.507	Lp E, Lp F, Lp A	Rajendran et al. (2024)
7	157.122	157.1223	C9H16O2H+	(Z)-whiskey lactone (β-methyl-γ-octalactone)	0.24	1.424	common	Yáñez-Serrano et al. (2021)
8	26.015	26.0151	C2H2+	alkyl fragment	0.989	1.03	common	Rajendran et al. (2025)
8	47.012	47.0127	CH2O2H+	formic acid	1.504	1.105	common	Yáñez-Serrano et al. (2021)
8	47.048	47.0491	C2H6OH+	ethanol	1.134	0.832	common	Rajendran et al. (2024)
8	57.034	57.0334	C3H4OH+	propionic acid fragment, 1-butanol fragment, hexanal fragment, hexenyl acetate or aldehyde fragment	0.078	0.181	common	(Rajendran et al., 2025; Yáñez-Serrano et al., 2021)
8	57.069	57.0698	C4H8H+	1-butanol fragment	0.803	0.687	common	Rajendran et al. (2024)
8	61.028	61.0289	C2H4O2H+	acetic acid*	1.23	0.909	common	Rajendran et al. (2024)

(*continued on next page*)

Table 1 (*continued*)

Dominant cycle	Measured mass	Theoretical mass	Protonated formula	Tentative identification	VIP_comp1	VIP_comp2	Strain specificity	Ref.
8	71.048	71.0491	C4H6OH+	2-butenal	0.6	0.452	Lp E	Yáñez-Serrano et al. (2021)
8	71.085	71.0855	C5H10H+	3-methyl-butanol fragment	0.758	0.682	common	Rajendran et al. (2024)
8	75.043	75.0446	C3H6O2H+	acetone alcohol*	0.446	0.468	common	
8	81.044	81.0452	C4H4N2H+	pyrazine*	0.136	0.289	common	Rajendran et al. (2024)
8	85.029	85.0284	C4H4O2H+	2(3H)-furanone	1.233	1.084	common	Yáñez-Serrano et al. (2021)
8	89.059	89.0597	C4H8O2H+	acetoin*, isobutyric acid*, butanoic acid*	0.868	0.625	Lp E	Yáñez-Serrano et al. (2021)
8	93.037	93.0368	C3H8OSH+	2-methyl-mercaptoethanol	1.077	0.98	common	Yáñez-Serrano et al. (2021)
8	99.044	99.0446	C5H6O2H+	2-furanmethanol	0.601	0.64	common	Yáñez-Serrano et al. (2021)
8	101.059	101.0597	C5H8O2H+	1-propen-2-ol acetate	0.263	0.319	common	
8	103.040	103.0389	C4H6O3H+	acetoacetic acid	1.387	1.042	common	
8	103.075	103.0753	C5H10O2H+	3-methyl-butanoic acid*	1.265	0.944	common	Yáñez-Serrano et al. (2021)
8	105.057	105.0546	C4H8O3H+	ester, hydroxy carboxilyc acid	0.034	0.785	Lp E, F and A	Yáñez-Serrano et al. (2021)
8	111.045	111.044	C6H6O2H+	1,2-benzenediol	0.657	0.711	common	Yáñez-Serrano et al. (2021)
8	113.061	113.0597	C6H8O2H+	5-methyl, 2-furanmethanol*	0.386	0.299	common	
8	115.039	115.0389	C5H6O3H+	5-hydroxymethyl-2(5H)-furanone	1.227	1.058	common	Yáñez-Serrano et al. (2021)
8	119.069	119.0702	C5H10O3H+	diethyl carbonate	1.141	0.826	common	Yáñez-Serrano et al. (2021)
8	121.051	121.0495	C4H8O4H+	n.i.	1.242	0.938	common	
8	131.071	131.0702	C6H10O3H+	ethyl acetoacetate	0.676	0.49	Lp E	Yáñez-Serrano et al. (2021)
8	153.129	153.1273	C10H16OH+	2,4-decadienal, monoterpenol	1.131	1.223	common	Yáñez-Serrano et al. (2021)
8	155.143	155.1435	C10H18OH+	oxygenated monoterpenes	0.557	1.882	common	Yáñez-Serrano et al. (2021)
8	173.157	173.1541	C10H20O2H+	decanoic acid*	1.426	1.288	common	(Rajendran et al., 2024, 2025)
8	191.162	191.1641	C10H22O3H+	n.i.	1.399	1.242	common	

fermentation cycles. In particular, m/z 71.048, m/z 87.046, m/z 89.059, m/z 91.024, m/z 131.071 and m/z 143.144 showed a clear late-stage accumulation in WCFS1, distinguishing this strain from the wine-associated isolates. This pattern was consistent with the multivariate separation observed in PCA and PLS-DA and indicates that the most evident strain-specific differences emerged during the late growth phase. Among the wine-associated strains, A and F showed closely related volatilome trajectories. This similarity was visible in the PCA (Fig. 1) and it was confirmed by several shared kinetic profiles, including m/z 97.101 (p.f. $C_7H_{12}H^+$, t.i. alkyl fragment), m/z 115.112 (p.f. $C_7H_{14}OH^+$, t.i. 2-heptanone), m/z 143.144 (p.f. $C_9H_{18}OH^+$, t.i. 2-nonanone), m/z 161.150 (p.f. $C_9H_{20}O_2H^+$, t.i. 1,9-nonanediol), m/z 169.159 (p.f. $C_{11}H_{20}OH^+$, t.i. 10-undecenal) and m/z 171.176 (p.f. $C_{11}H_{22}OH^+$, t.i. as 2-undecanone). Strains B and D also showed comparable behaviour, especially for m/z 115.077 (p.f. $C_6H_{10}O_2H^+$, t.i. as 2,5-hexanedione), which increased until cycle 3 and subsequently decreased. Strain C showed an intermediate profile, resembling strains B and D in the early cycles but diverging in the later stages. Additional strain-specific signals were observed among the wine-associated isolates. Strains A and F showed similar trends for m/z 45.034, t.i. as acetaldehyde (p.f. $C_2H_4OH^+$). Strain F showed distinctive behaviour for m/z 111.117, tentatively assigned to a hydrocarbon group, and m/z 129.127, t.i. as 1-octen-3-ol. Strain A showed a specific trend for m/z 34.995, t.i. as hydrogen sulfide (p.f. H_2SH^+). These signals contributed to the secondary differentiation among the wine strains, although their separation was less pronounced than that observed for WCFS1. Overall, the PTR-ToF-MS results revealed a dominant time-dependent evolution of the volatilome common to all *L. plantarum* strains, accompanied by strain-specific differences. The reference strain WCFS1 showed the most distinctive volatilome, particularly during the late fermentation cycles, whereas the wine-associated strains displayed partially overlapping profiles, with A/F and B/D forming the most evident pairs of similar behaviour.

4. Discussion

The present study provides an online description of the evolution of the volatilome of *L. plantarum* during growth in MRS medium, with particular emphasis on the reference strain WCFS1. The results show that VOC production is shaped by three interconnected factors: fermentation time, substrate composition, and strain identity. The temporal component was the dominant driver of variation, as shown by PCA and PLS-DA, whereas the strain-dependent component became particularly evident for WCFS1 during the late growth phase. This behaviour is consistent with the high metabolic versatility of *L. plantarum*, a species capable of colonising diverse ecological niches and redirecting carbon fluxes in response to substrate availability and environmental conditions (Kleerebezem et al., 2003; Martino et al., 2016; Zheng et al., 2020). In this context, microbial VOCs can be considered dynamic biomarkers of physiological state, substrate transformation, and strain-specific metabolic potential (Khomenko et al., 2017; Weisskopf et al., 2021). The experimental results are consistent with the hypothesis that the observed volatilome reflects metabolites commonly associated with central carbon metabolism, amino acid catabolism, lipid transformation, and, in plant matrices, terpenoid biotransformation (Corvino, Spano, et al., 2026), although these metabolic origins were not directly investigated in the present study. The volatilome did not behave as a static strain fingerprint but rather as a dynamic metabolic output linked to the bacterial growth phase, supporting the relevance of volatilomics as an 'omic' strategy for providing a temporal dimension to the study of bacterial phenomena (Meredith & Tfaily, 2022). This finding is consistent with LAB fermentation

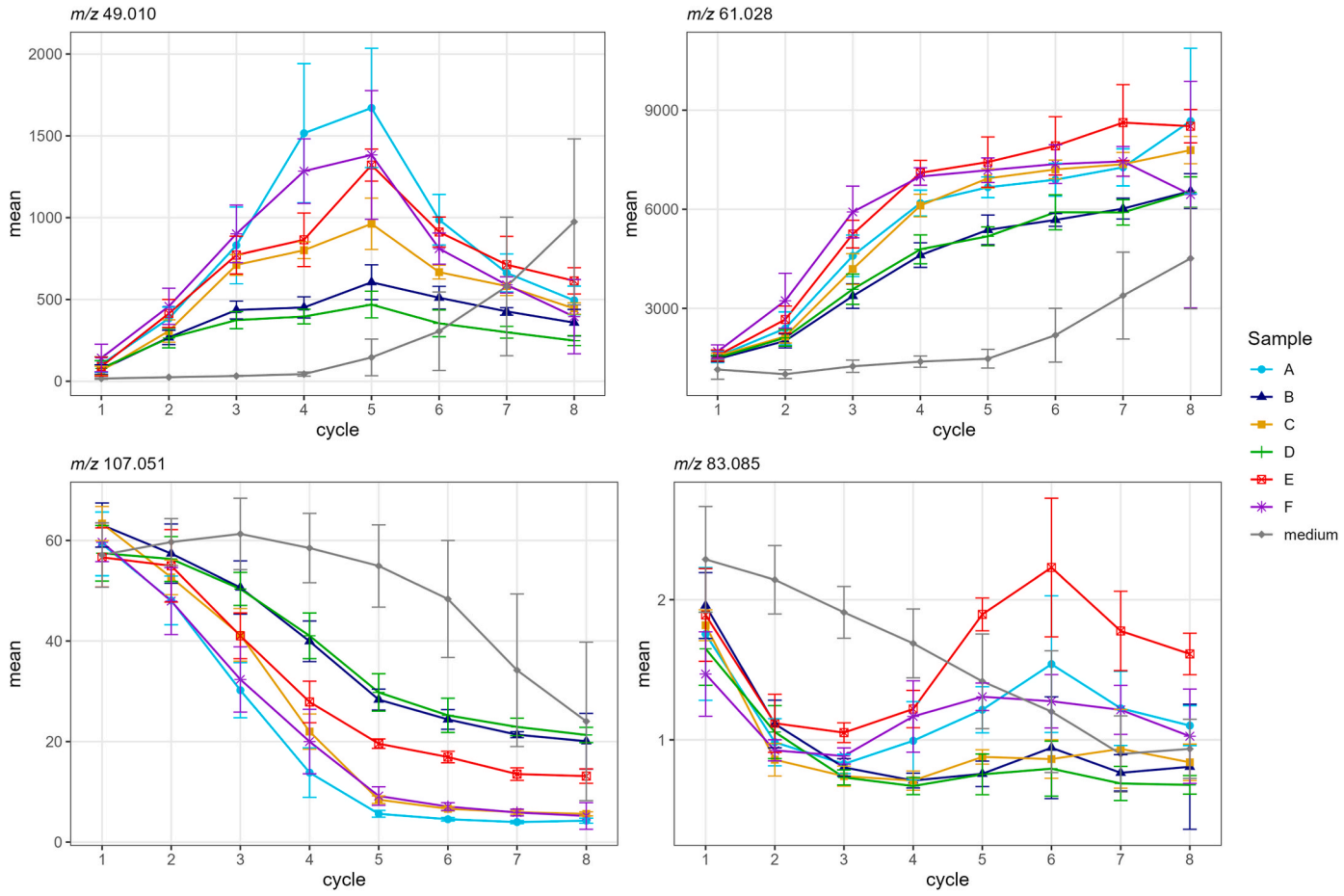


Fig. 3. Temporal evolution of selected PTR-ToF-MS ions representative of the main VOC kinetic profiles observed during growth of *Lactiplantibacillus plantarum* strains in MRS medium. Mean ion intensities are plotted across fermentation cycles 1–8 for strains A–F and the uninoculated medium control; error bars indicate variability among replicates.

physiology: during early growth, cells adapt to the medium and consume readily available substrates, while during exponential and stationary phases, they progressively redirect metabolism toward secondary routes, including amino acid conversion, redox-balancing pathways, and organic acid production. Previous studies have shown that *L. plantarum* can switch between homofermentative and heterofermentative metabolism depending on substrate composition and environmental conditions (Zheng et al., 2020). Under typical carbohydrate-rich conditions, carbon flux is mainly directed toward lactate through the Embden–Meyerhof–Parnas pathway, whereas alternative pyruvate-dissipating routes can generate volatile metabolites such as acetoin, diacetyl, acetaldehyde, ethanol, acetic acid, and carbon dioxide (Axelsson, 2004; Hang et al., 2026; Marathe & Ghosh, 2009). This metabolic flexibility may explain why several VOCs were progressively accumulated during the intermediate and late fermentation cycles.

The four kinetic profiles identified in Fig. 3 indicate the volatilome of *L. plantarum* in MRS medium reflects a succession of metabolic states rather than a single fermentation endpoint. A critical aspect of this study is the use of MRS medium as a controlled microbiological substrate. MRS is specifically formulated to support the growth of lactobacilli and contains glucose as the main carbon source, along with peptone, yeast extract, Lab-Lemco powder, salts, and growth factors (Hayek et al., 2019; Man et al., 1960). This composition provides fermentable carbohydrates, amino acids, peptides, nucleic acid derivatives, minerals, and vitamins, all of which can act as direct or indirect precursors of volatile metabolites. For this reason, the volatilome detected in the present study should not be interpreted as a direct equivalent of the aroma profile produced in food matrices such as wine, dairy products, vegetables, or cereals. Rather, it represents a controlled physiological volatilome, useful for comparing strain behaviour under standardised growth conditions. This distinction is important because the volatile performance of *L. plantarum* is highly matrix-dependent. The same species may increase aldehyde levels in dairy, meat, or cereal matrices, while reducing them in fruit juices and plant-based milk alternatives, depending on precursor availability, redox conditions, and strain-specific enzymatic activities (Corvino, Spano, et al., 2026; Shahidi & Hossain, 2022; Xing et al., 2025). Pyrazine-related signals further illustrate the importance of medium control. Pyrazines are typically associated with thermal processing and Maillard reactions, which occur at high temperatures and involve reducing sugars and amino compounds (Chen et al., 2024). Their relatively flat trends across inoculated samples and their occurrence in the uninoculated medium suggest that they were more likely linked to medium preparation or sterilisation than to active bacterial metabolism. Nevertheless, pyrazines may also originate from fermentation intermediates, such as acetoin, via condensation reactions (Weisskopf et al., 2021). Therefore, these compounds should be interpreted cautiously, particularly when they are present in both inoculated and uninoculated controls. Among the shared VOCs, acetic acid is a key marker of *L. plantarum* fermentative activity. In the present study, the ion at m/z 61.028, tentatively assigned to acetic acid, increased during fermentation and was confirmed by GC-MS analysis. This result aligns with previous evidence indicating that acetic acid, together with acetoin, is among the most recurrent volatile markers of *L. plantarum* across different fermented matrices (Corvino, Spano, et al., 2026; Xing et al., 2025). Acetic acid may be derived from carbohydrate metabolism via

the acetyl-CoA or phosphoketolase pathways, particularly when cells redirect carbon flux towards acetate formation for redox balancing or energy conservation. In LAB, pyruvate serves as a central metabolic node, connecting primary carbohydrate metabolism to aroma-active compounds. Under fermentative conditions, pyruvate is primarily converted to lactate, but it can also be diverted toward α-acetolactate, acetoin, diacetyl, acetaldehyde, ethanol, formate, acetate, and CO_2 (Axelsson, 2004; Hang et al., 2026; Marathe & Ghosh, 2009). The balance among these routes is influenced by pH, redox status, substrate composition, oxygen availability, and strain-specific enzymatic equipment. Diacetyl and acetoin are especially relevant because they are widely associated with buttery and creamy sensory notes in fermented foods, although excessive diacetyl may lead to an undesirable flavor imbalance (Hang et al., 2026; Smid & Kleerebezem, 2014). The detection of m/z 87.046, t.i.as 2,3-butanedione/diacetyl and m/z 89.059, t.i. as acetoin/isobutyric acid/butanoic acid is consistent with pyruvate-derived metabolism. Diacetyl can arise from the spontaneous oxidative decarboxylation of α-acetolactate, whereas the enzymatic decarboxylation of α-acetolactate can produce acetoin and may subsequently be reduced to 2,3-butanediol. These pathways also contribute to redox regulation and intracellular pH homeostasis, as converting pyruvate into neutral compounds may help balance metabolism under acidic or pyruvate-accumulating conditions (Hang et al., 2026; Jyoti et al., 2003). In this study, the late accumulation of these ions, particularly in *Lp* WCFS1, suggests a greater contribution of pyruvate-derived VOC during the transition to the stationary phase, although the underlying metabolic pathways were not directly investigated. Interpretation of m/z 89.059 requires caution because PTR-ToF-MS cannot fully discriminate between isomers. The same nominal ion may include contributions from acetoin, isobutyric acid, and butanoic acid, all of which were relevant to the GC-MS-supported interpretation. This confirms the importance of GC-MS as a complementary technique for resolving ambiguities in PTR-ToF-MS. Butanoic acid may originate from carbohydrate fermentation or from the transformation of short-chain fatty acid precursors present in complex medium components. Short- and medium-chain organic acids are relevant in food systems because they contribute to acidification and antimicrobial activity, thereby influencing both safety and sensory profile (Özcelik et al., 2016). Several compounds exhibiting a profile C trend are consistent with the consumption or transformation of amino acid-derived volatiles. Benzaldehyde, identified at m/z 107.051 and confirmed by GC-MS, decreased during fermentation. It can arise from the catabolism of aromatic amino acids, particularly phenylalanine and tyrosine, via transamination to the corresponding α-keto acids, followed by chemical or enzymatic conversion (Sgarbi et al., 2013). The role of manganese in the conversion of phenylpyruvic acid to benzaldehyde has also been reported in LAB-related systems (Nierop Groot & de Bont, 1999). In the present study, the decrease in benzaldehyde may indicate microbial transformation, reduction, or further conversion into other derivatives during growth. Branched-chain aldehydes and alcohols also contributed to the early-stage volatilome. The ion m/z 87.080 t.i. as to 2-methylbutanal/3-methylbutanal, and m/z 89.087, t.i.as 3-methyl-1-butanol, showed decreasing trends. These compounds are typically associated with branched-chain amino acid catabolism. Leucine, isoleucine, and valine are first transaminated to α-keto acids and then decarboxylated to branched-chain aldehydes, which can be further reduced to the corresponding alcohols or oxidised to acids (Ardö, 2006; Liu et al., 2008). Leucine catabolism yields 3-methylbutanal and 3-methyl-1-butanol, whereas isoleucine and valine generate 2-methylbutanal and 2-methylpropanal. These compounds can contribute malty, fruity, cheesy, or fermented notes depending on concentration and matrix. The decrease observed for these ions suggests that early VOCs may have been progressively converted into downstream metabolites rather than continuously accumulated. For example, branched-chain alcohols may participate in ester formation when suitable acid precursors and esterase activity are available. Ester accumulation in *L. plantarum* is often time-dependent and requires sufficient availability of both alcohol and acid precursors (Bai et al., 2023; Huang et al., 2025). Although ester formation was not the dominant feature of growth in MRS medium, decreases in selected alcohols and aldehydes are consistent with their involvement in further biotransformation pathways. Sulfur-containing VOCs were an important component of the volatilome, particularly in profiles associated with mid-fermentation changes. The ion m/z 49.010, t.i.as methanethiol, increased until approximately cycle 5 and then decreased. Methanethiol is a central intermediate in microbial sulfur metabolism and can be generated from the catabolism of methionine and cysteine (Liu et al., 2008; Weisskopf et al., 2021). It can undergo further transformations to produce dimethyl sulfide, dimethyl disulfide, dimethyl trisulfide, and thioesters, depending on redox conditions and substrate availability. The transient nature of methanethiol in this study is biologically plausible, as this compound is reactive and can be oxidised or converted into other sulfur derivatives. Oxidative dimerisation or transformation into dimethyl sulfide-like compounds may explain the observed decline after the central fermentation phase. The detection of m/z 91.024, t.i. as methylthioacetate, particularly in strain E (*Lp* WCFS1), is consistent with the involvement of sulfur-related pathways previously described in the literature. Methylthioacetate and related thioesters may be generated through the reaction of methanethiol with acyl-CoA-derived short-chain acid moieties, as described for sulfur aroma pathways in fermented foods (Landaud et al., 2008). Sulfur VOCs are technologically important because they can contribute positively or negatively to food aroma depending on concentration and matrix. In cheese, beer, and wine, low concentrations of sulfur compounds can add complexity, whereas excessive accumulation can generate cabbage-, garlic-, or rotten-egg-like, or other off-odors (Landaud et al., 2008; Rajendran et al., 2024). In the present study, the specific peak of m/z 34.995, t.i. as hydrogen sulfide, was particularly evident in strain A around cycle 5. This suggests differences in sulfur-related metabolism among the strains under the tested conditions. From an oenological perspective, this signal deserves attention because hydrogen sulfide is generally considered a negative aroma compound in wine due to its low odor threshold and sulfurous character (although bioproduction under oenological conditions needs to be verified). A distinctive feature of *Lp* WCFS1 was the accumulation of several compounds tentatively linked to lipid transformation, including methyl ketones and long-chain carbonyls. The ions at m/z 115.112, 143.144, and 171.176, t.i.as 2-heptanone, 2-nonanone, and 2-undecanone, respectively, showed strain-dependent late-stage accumulation, with WCFS1 exhibiting the highest values for several of these signals. Methyl ketones can arise from β-oxidation and decarboxylation of β-ketoacids formed during fatty acid metabolism, although thermal degradation and Maillard-associated pathways may also contribute in complex matrices (Dan et al., 2019; Tian et al., 2025; Zhang et al., 2024). In food systems, methyl ketones are important aroma-active compounds. In dairy products, 2-heptanone and 2-nonanone are often associated with fermented, cheesy, or creamy notes and have been reported as strain-dependent metabolites in *L. plantarum*-fermented products (Tian et al., 2025; Zhang et al., 2024). However, their sensory significance is matrix-dependent. In some matrices, they contribute positively to aroma complexity, whereas in others they may be associated with spoilage or heat-treatment markers (Avalli et al., 2004; Yang et al., 2025). In this study, because MRS contains complex nitrogen sources and small amounts of lipid-related precursors from yeast extract and Lab-Lemco, the accumulation of methyl ketones should be interpreted as evidence of metabolic potential rather than as a direct predictor of food aroma. The detection of long-chain aldehydes, alcohols, and diols, including m/z 169.159 t.i. as 10-undecenal, m/z 161.150 t.i. as 1,9-nonanediol, and m/z 189.181 t.i. as 1,11-undecanediol, also points to lipid-related or carbonyl-reduction pathways. This evidence may reflect the ability of *L. plantarum* in transforming lipid-derived aldehydes into alcohols via oxidoreductase activity (Shahidi & Hossain, 2022; Xing et al., 2025). Nevertheless, the tentative assignments of some of these compounds should be treated

with caution, particularly where direct evidence of LAB production is limited. The most relevant strain-dependent result of this study was the clear differentiation of *Lp* WCFS1 from the five wine-associated strains. PCA showed that strain E (*Lp* WCFS1) followed a distinct trajectory, especially during late fermentation, while the selected VOC kinetics confirmed that *Lp* WCFS1 accumulated several ions at higher levels than the other strains. These included m/z 71.048, m/z 87.046, m/z 89.059, m/z 91.024, m/z 131.071, m/z 143.144, m/z 169.159 and m/z 171.176. This pattern indicates that *Lp* WCFS1 differed not only in the amount of VOCs released but also in the timing of volatile accumulation. The late-stage increase of diacetyl/acetoin-related ions suggests the possible stronger activation of pyruvate-dissipating pathways in *Lp* WCFS1. Similarly, the accumulation of methylthioacetate-like and methyl ketone-like signals suggests a possible contribution of sulfur amino acid catabolism and lipid-derived pathways to the *Lp* WCFS1-specific volatilome. This broader late-stage VOC repertoire may reflect strain-specific enzymatic machinery, redox-balancing strategies, or adaptations to nutrient limitation during the transition to the stationary phase. From an ecological perspective, this behaviour may be related to the different origin of *Lp* WCFS1. Unlike strains A, B, C, D, and F, which are wine-associated and selected for oenological/pro-technological traits, E (*Lp* WCFS1) was originally isolated from human saliva. *L. plantarum* is often described as a nomadic species, capable of colonising diverse ecological niches because of its relatively large genome and flexible metabolic repertoire (Kleerebezem et al., 2003; Martino et al., 2016). Therefore, the distinctive volatilome of *Lp* WCFS1 may reflect differences in adaptive background compared with that of wine-selected strains. However, this interpretation should be approached with caution: the present study demonstrates strain-dependent volatilome behaviour under standardised MRS conditions, but further experiments in wine- and saliva-like matrices would be needed to directly link these VOC patterns to ecological adaptation. Although *Lp* WCFS1 was the main focus, the five wine-associated strains also displayed relevant patterns. Groupings wine-associated *L. plantarum* strains suggest that they may share partially convergent volatilomes, although each isolate retains specific traits. From an oenological perspective, two findings are particularly relevant. First, strains A and F showed an increasing trend at m/z 45.034, t.i. as acetaldehyde. Acetaldehyde is a key wine-related metabolite because it can participate in reactions with anthocyanins, contributing to the formation of pyranoanthocyanins and potentially improving colour stability (Wang et al., 2018). In addition, its concentration requires careful monitoring, as above its sensory threshold it can impart an unpleasant, pungent aroma (Dan et al., 2019). However, acetaldehyde production in *L. plantarum* is not constitutive and appears to be strain-specific, as also emphasised in the literature (Dan et al., 2019; Tian et al., 2025). Therefore, the behaviour of strains A and F may be relevant for future screening in wine-like systems. Second, strain A showed a transient accumulation of m/z 34.995, t.i. as hydrogen sulfide. This finding is relevant because H_2S is undesirable in wine and other fermented beverages due to its rotten-egg and sulfurous notes. Its transient accumulation suggests that sulfur amino acid catabolism or sulfur reduction pathways may be particularly active in this strain under the tested conditions (Rankine, 1963; Weisskopf et al., 2021). Although the MRS system cannot directly predict wine performance, this result suggests that sulfur VOC monitoring deserves further investigation as a potential screening tool for wine-associated *L. plantarum* strains before validation in real fermentation matrices. This study confirms the value of PTR-ToF-MS for online monitoring microbial volatilome dynamics. The technique enabled rapid, repeated, and non-invasive analysis of VOC evolution across eight fermentation cycles, providing temporal information that would be difficult to obtain with conventional offline methods alone. This is particularly useful in fermentation studies because VOCs are transient and may peak or decline within specific growth phases, as shown here for methanethiol, benzaldehyde, and several *Lp* WCFS1-associated late-stage compounds. Overall, the present study provides evidence that online volatilomics can capture growth-phase- and strain-dependent metabolic features of *L. plantarum*. Under standardised MRS conditions, the species displayed a shared temporal volatilome, characterised by early depletion of medium-associated compounds, mid-fermentation accumulation of signals related to sulfur and organic acids, and late-stage formation of pyruvate-, amino acid-, and lipid-derived VOCs. Within this common framework, *Lp* WCFS1 displayed the most distinctive late-stage volatilome, characterised by greater accumulation of diacetyl/acetoin-related signals, methyl ketones, sulfur-associated compounds, and selected ester-like or long-chain carbonyl compounds. At the same time, the comparison with wine-associated strains under controlled MRS conditions highlights the importance of strain selection for flavour-related applications, although these observations require validation in real fermentation matrices. The results also confirm that VOC profiles should not be generalised at the species level: even under identical growth conditions, *L. plantarum* strains can differ markedly in timing, intensity, and chemical nature of volatile production.

5. Conclusions

This study provides an online characterisation of the volatilome dynamics of *L. plantarum* WCFS1 during growth in MRS medium using PTR-ToF-MS and a direct comparison with five wine-associated *L. plantarum* strains under standardised fermentation conditions. Fermentation stage primarily drove volatile production, with distinct temporal patterns emerging from early to late fermentation. Within this common temporal pattern, *Lp* WCFS1 displayed the most distinctive volatilome, particularly through the late accumulation of pyruvate-derived compounds, sulfur-related metabolites, methyl ketones, and long-chain carbonyl compounds. The comparative analysis showed partially convergent volatilome profiles among wine-selected strains under controlled MRS conditions, while overall volatile production remained strain-dependent. Methodologically, the study demonstrates the effectiveness of PTR-ToF-MS as a rapid, online approach for monitoring microbial volatilome dynamics, while highlighting the complementary role of GC-MS for metabolite annotation and interpretation. Future investigations in food-relevant matrices will be necessary to determine whether the strain-specific signatures observed under these experimental conditions are maintained. More broadly, the volatilomic characterization of *Lactiplantibacillus plantarum* represents a promising approach for investigating metabolic functions of different strains and their potential contribution to the quality, aroma, and development of fermented foods.

CRediT authorship contribution statement

Antonia Corvino: Writing – original draft, Software, Methodology, Investigation, Formal analysis, Data curation. **Emanuela Betta:** Writing – review & editing, Software, Methodology, Data curation. **Iuliia Khomenko:** Writing – review & editing, Software, Methodology, Data curation. **Vittorio Capozzi:** Writing – review & editing, Supervision, Resources, Project administration, Investigation, Funding acquisition, Conceptualization. **Franco Biasioli:** Writing – review & editing, Validation, Supervision, Resources, Project administration, Investigation, Funding acquisition, Conceptualization. **Mariagiovanna Fragasso:** Writing – original draft, Visualization, Validation, Supervision, Methodology, Investigation, Formal analysis, Conceptualization.

Declaration of competing interests

The authors declare that they have no known competing financial interests or personal relationships that could have appeared to influence the work reported in this paper.

The author is an Editorial Board Member/Editor-in-Chief/Associate Editor/Guest Editor for this journal and was not involved in the editorial review or the decision to publish this article.

Acknowledgements

This work is supported by the project “SpeedyFermHub: Knowledge HUB for SPEEDY characterisation, optimisation and scale-up of FERMented, plant-based new foods improving resilience of European Food Systems” (ID 215), funded by the 1st call of the ‘Partnership cofund FutureFoodS’. Antonia Corvino was supported by the project "Interconnected Nord-Est Innovation Ecosystem (iNEST) " funded from the European Union Next-GenerationEU (PIANO NAZIONALE DI RIPRESA E RESILIENZA (PNRR)—MISSIONE 4 COMPONENTE 2, INVESTIMENTO 1.5—D.D. 1058 23/06/2022, ECS00000043).

Appendix A. Supplementary data

Supplementary data to this article can be found online at https://doi.org/10.1016/j.fbio.2026.110224.

Data availability

Data will be made available on request.

References

Abedin, M. M., Chourasia, R., Phukon, L. C., Sarkar, P., Ray, R. C., Singh, S. P., & Rai, A. K. (2024). Lactic acid bacteria in the functional food industry: Biotechnological properties and potential applications. *Critical Reviews in Food Science and Nutrition, 64*, 10730–10748. https://doi.org/10.1080/10408398.2023.2227896

Aljohani, A., Rashwan, N., Vasani, S., Alkhawashki, A., Wu, T. T., Lu, X., Castillo, D. A., & Xiao, J. (2025). The health benefits of probiotic *Lactiplantibacillus plantarum*: A systematic review and meta-analysis. *Probiotics and Antimicrobial Proteins, 17*, 3358–3377. https://doi.org/10.1007/s12602-024-10287-3

Ardö, Y. (2006). Flavour formation by amino acid catabolism. *Biotechnology Advances, 24*, 238–242. https://doi.org/10.1016/j.biotechadv.2005.11.005

Avalli, A., Povolo, M., Carminati, D., & Contarini, G. (2004). Significance of 2-heptanone in evaluating the effect of microfiltration/pasteurisation applied to goats' milk. *International Dairy Journal, 14*, 915–921. https://doi.org/10.1016/j.idairyj.2004.03.004

Axelsson, L. (2004). Lactic acid bacteria: Classification and physiology. *Food Science and Technology-New York-Marcel Dekker-, 139*, 1–66.

Bai, W., Mai, R., Guo, S., Li, X., Zhao, W., & Yang, J. (2023). The contribution of inoculated probiotics to increased protein-derived volatile flavor compounds. *Food Research International, 174*, Article 113629. https://doi.org/10.1016/j.foodres.2023.113629

Banicod, R. J. S., Tabassum, N., Javaid, A., Kim, Y.-M., & Khan, F. (2026). Lactic acid bacteria–derived secondary metabolites: Emerging natural alternatives for food preservation. *Probiotics and Antimicrobial Proteins, 18*, 3113–3150. https://doi.org/10.1007/s12602-025-10672-6

Cappellin, L., Biasioli, F., Granitto, P. M., Schuhfried, E., Soukoulis, C., Costa, F., Märk, T. D., & Gasperi, F. (2011). On data analysis in PTR-TOF-MS: From raw spectra to data mining. *Sensors and Actuators B: Chemical, 155*, 183–190.

Chen, X., Li, Z., Lan, W., Sun, H., Chen, K., & Zhao, L. (2024). Maillard reaction products of hydrolyzed *Copyinds comatus* protein with various sugar-amino acid combinations: Focusing on their meaty aroma notes and salt reduction abilities. *Food Bioscience*, Article 104503.

Cirat, R., Capozzi, V., Benmechernene, Z., Spano, G., Grieco, F., & Fragasso, M. (2024). LAB antagonistic activities and their significance in food biotechnology: Molecular mechanisms, food targets, and other related traits of interest. *Fermentation, 10*, 222. https://doi.org/10.3390/fermentation10040222

Corvino, A., Khomenko, I., Betta, E., Capozzi, V., & Biasioli, F. (2026). Volatilomics analysis of table olive ‘Bella di Cerignola’ PDO and associated brines: a case study on different fermentation styles and olive sizes. *Measurement: Food, 22*, Article 100287. https://doi.org/10.1016/j.meafoo.2026.100287

Corvino, A., Silcock, P., Capozzi, V., & Biasioli, F. (2024). Emerging evidence on the potential of PTR - MS as rapid, direct and high-sensitivity sensors to promote innovation in the fermented beverages sector. *International Journal of Food Science and Technology, 59*, 8434–8444. https://doi.org/10.1111/ijfs.17398

Corvino, A., Spano, G., Biasioli, F., & Capozzi, V. (2026). The aromatic footprint of *Lactiplantibacillus plantarum*: Volatilome intraspecific diversity and variability across food matrices. *Trends in Food Science & Technology*, Article 106076.

Dan, T., Chen, H., Li, T., Tian, J., Ren, W., Zhang, H., & Sun, T. (2019). Influence of *Lactobacillus plantarum* P-8 on fermented milk flavor and storage stability. *Frontiers in Microbiology, 9*.

Deng, L., Zhao, X., & Chen, L. (2025). Microbial volatile organic compounds for food quality and safety: Metabolic pathways, sampling and detection, and machine learning-driven insights. *Trends in Food Science & Technology, 166*, Article 105414. https://doi.org/10.1016/j.tifs.2025.105414

Hang, S., Yu, H., Chen, C., Ge, C., & Tian, H. (2026). Strain-specific mechanisms of enhanced diacetyl biosynthesis in *Lactiplantibacillus plantarum* unveiled by multi-omics integration. *International Journal of Food Microbiology, 453*, Article 111691. https://doi.org/10.1016/j.ijfoodmicro.2026.111691

Hayek, S. A., Gyawali, R., Aljaloud, S. O., Krastanov, A., & Ibrahim, S. A. (2019). Cultivation media for lactic acid bacteria used in dairy products. *Journal of Dairy Research, 86*, 490–502. https://doi.org/10.1017/S002202991900075X

Huang, J., Chen, J., & Li, X. (2025). Preliminary study on the application of protease-producing *Lactiplantibacillus plantarum* in yogurt fermentation. *Fermentation, 11*, 215. https://doi.org/10.3390/fermentation11040215

Jo, D.-M., Ko, S.-C., Kim, K. W., Yang, D., Kim, J.-Y., Oh, G.-W., Choi, G., Lee, D.-S., Tabassum, N., Kim, Y.-M., & Khan, F. (2025). Artificial intelligence-driven strategies to enhance the application of lactic acid bacteria as functional probiotics: Health promotion and optimization for industrial applications. *Trends in Food Science & Technology, 165*, Article 105309. https://doi.org/10.1016/j.tifs.2025.105309

Jyoti, B. D., Suresh, A. K., & Venkatesh, K. V. (2003). Diacetyl production and growth of *Lactobacillus rhamnosus* on multiple substrates. *World Journal of Microbiology and Biotechnology, 19*, 509–514. https://doi.org/10.1023/A:1025170630905

Khomenko, I., Stefanini, I., Cappellin, L., Cappelletti, V., Franceschi, P., Cavalieri, D., Märk, T. D., & Biasioli, F. (2017). Non-invasive real time monitoring of yeast volatilome by PTR-ToF-MS. *Metabolomics, 13*, 118. https://doi.org/10.1007/s11306-017-1259-y

Kleerebezem, M., Boekhorst, J., Van Kranenburg, R., Molenaar, D., Kuipers, O. P., Leer, R., Tarchini, R., Peters, S. A., Sandbrink, H. M., & Fiers, M. W. (2003). Complete genome sequence of *Lactobacillus plantarum* WCFS1. *Proceedings of the National Academy of Sciences, 100*, 1990–1995.

Landaud, S., Helinck, S., & Bonnarme, P. (2008). Formation of volatile sulfur compounds and metabolism of methionine and other sulfur compounds in fermented food. *Applied Microbiology and Biotechnology, 77*, 1191–1205. https://doi.org/10.1007/s00253-007-1288-y

Li, Q., Zeng, X., Fu, H., Wang, X., Guo, X., & Wang, M. (2023). *Lactiplantibacillus plantarum*: A comprehensive review of its antifungal and anti-mycotoxic effects. *Trends in Food Science & Technology, 136*, 224–238. https://doi.org/10.1016/j.tifs.2023.04.019

Liu, M., Nauta, A., Francke, C., & Siezen, R. J. (2008). Comparative genomics of enzymes in flavor-forming pathways from amino acids in lactic acid bacteria. *Applied and Environmental Microbiology, 74*, 4590–4600. https://doi.org/10.1128/AEM.00150-08

Makhoul, S., Romano, A., Cappellin, L., Spano, G., Capozzi, V., Benozzi, E., Märk, T. D., Aprea, E., Gasperi, F., & El-Nakat, H. (2014). Proton-transfer-reaction mass spectrometry for the study of the production of volatile compounds by bakery yeast starters. *Journal of Mass Spectrometry, 49*, 850–859.

Man, J. C. D., Rogosa, M., & Sharpe, M. E. (1960). A medium for the cultivation of lactobacilli. *Journal of Applied Bacteriology, 23*, 130–135. https://doi.org/10.1111/j.1365-2672.1960.tb00188.x

Marathe, M., & Ghosh, J. (2009). Study of proteinase activity of *Lactobacillus plantarum* NCIM 2083. *International Journal of Genetics and Molecular Biology, 1*, 1–5.

Martino, M. E., Bayjanov, J. R., Caffrey, B. E., Wels, M., Joncour, P., Hughes, S., Gillet, B., Kleerebezem, M., van Hijum, S. A. F. T., & Leulier, F. (2016). Nomadic lifestyle of *Lactobacillus plantarum* revealed by comparative genomics of 54 strains isolated from different habitats. *Environmental Microbiology, 18*, 4974–4989. https://doi.org/10.1111/1462-2920.13455

Mazzucotelli, M., Farneti, B., Khomenko, I., Gonzalez-Estanol, K., Pedrotti, M., Fragasso, M., Capozzi, V., & Biasioli, F. (2022). Proton transfer reaction mass spectrometry: A green alternative for food volatilome profiling. *Green Analytical Chemistry, 3*, Article 100041. https://doi.org/10.1016/j.greeac.2022.100041

Meredith, L. K., & Tfaily, M. M. (2022). Capturing the microbial volatilome: An oft overlooked “ome.”. *Trends in Microbiology, 30*, 622–631. https://doi.org/10.1016/j.tim.2021.12.004

Montagano, F., Prete, R., Fanti, F., Dell'Orco, F., Oliva, E., Compagnone, D., & Corsetti, A. (2025). Enrichment of γ-aminobutyric acid (GABA) in a legume-based beverage through the fermentation by *Lactiplantibacillus plantarum*. *Current Research in Food Science, 11*, Article 101176. https://doi.org/10.1016/j.crfs.2025.101176

Moretton, M., Khomenko, I., Cunedioğlu, H., Spano, G., Capozzi, V., Biasioli, F., & Fragasso, M. (2025). Comparative volatilome profiling of milk kefir and cereal-based kefir analogues fermented with milk and water kefir grains. *Food Bioscience, 74*, Article 107731. https://doi.org/10.1016/j.fbio.2025.107731

Nierop Groot, M. N., & de Bont, J. A. M. (1999). Involvement of manganese in conversion of phenylalanine to benzaldehyde by lactic acid bacteria. *Applied and Environmental Microbiology, 65*, 5590–5593. https://doi.org/10.1128/AEM.65.12.5590-5593.1999

Özcelik, S., Kuley, E., & Özogul, F. (2016). Formation of lactic, acetic, succinic, propionic, formic and butyric acid by lactic acid bacteria. *LWT, 73*, 536–542. https://doi.org/10.1016/j.lwt.2016.06.066

Presutto, E., Capozzi, V., de Chiara, M. L. V., Drider, D., Spano, G., & Fragasso, M. (2026). Exploring lactic acid bacteria from fresh fruits, vegetables, and edible flowers: From biodiversity valorisation to food applications. *World Journal of Microbiology and Biotechnology, 42*, 117. https://doi.org/10.1007/s11274-026-04872-7

Qian, M., Liang, Q., Zhao, B., Cheng, X., & Zhang, Y. (2026). Exopolysaccharides from Co-cultured *Lactiplantibacillus plantarum*: Structural properties and genetic basis for food hydrocolloid applications. *Food Hydrocolloids, 175*, Article 112516. https://doi.org/10.1016/j.foodhyd.2026.112516

Rajendran, S., Khomenko, I., Silcock, P., Betta, E., Biasioli, F., & Bremer, P. (2024). Impact of different carbon sources on volatile organic compounds (VOCs) produced during fermentation by *Levilactobacillus brevis* WLP672 measured using proton transfer reaction time-of-flight mass spectrometry (PTR-ToF-MS). *Molecules, 29*, 3275. https://doi.org/10.3390/molecules29143275

Rajendran, S., Khomenko, I., Silcock, P., Betta, E., Biasioli, F., & Bremer, P. (2025). The use of proton-transfer-reaction time-of-flight mass spectrometry (PTR-ToF-MS) to

determine the volatile organic compounds (VOCs) produced by different lactic acid bacterial strains growing in defined media. *Applied Microbiology, 5*, 33.

Rankine, B. C. (1963). Nature, origin and prevention of hydrogen sulphide aroma in wines. *Journal of the Science of Food and Agriculture, 14*, 79–91. https://doi.org/10.1002/jsfa.2740140204

Sgarbi, E., Lazzi, C., Tabanelli, G., Gatti, M., Neviani, E., & Gardini, F. (2013). Nonstarter lactic acid bacteria volatilomes produced using cheese components. *Journal of Dairy Science, 96*, 4223–4234. https://doi.org/10.3168/jds.2012-6472

Shahidi, F., & Hossain, A. (2022). Role of lipids in food flavor generation. *Molecules, 27*, 5014. https://doi.org/10.3390/molecules27155014

Smid, E. J., & Kleerebezem, M. (2014). Production of aroma compounds in lactic fermentations. *Annual Review of Food Science and Technology, 5*, 313–326. https://doi.org/10.1146/annurev-food-030713-092339

Teusink, B., Wiersma, A., Molenaar, D., Francke, C., Vos, W. M. de, Siezen, R. J., & Smid, E. J. (2006). Analysis of growth of *Lactobacillus plantarum* WCFS1 on a complex medium using a genome-scale metabolic model. *Journal of Biological Chemistry, 281*, 40041–40048. https://doi.org/10.1074/jbc.M606263200

Tian, H., Hang, S., Huang, N., Yu, H., Chen, C., & Ge, C. (2025). Strain-level variation in diacetyl production by *Lactiplantibacillus plantarum* reveals genetic drivers of flavor in fermented dairy. *Journal of Dairy Science, 108*, 10689–10699. https://doi.org/10.3168/jds.2025-27128

van den Nieuwboer, M., van Hemert, S., Claassen, E., & de Vos, W. M. (2016). *Lactobacillus plantarum* WCFS1 and its host interaction: A dozen years after the genome. *Microbial Biotechnology, 9*, 452–465. https://doi.org/10.1111/1751-7915.12368

Wang, S., Li, S., Zhao, H., Gu, P., Chen, Y., Zhang, B., & Zhu, B. (2018). Acetaldehyde released by *Lactobacillus plantarum* enhances accumulation of pyranoanthocyanins in wine during malolactic fermentation. *Food Research International, 108*, 254–263. https://doi.org/10.1016/j.foodres.2018.03.032

Weisskopf, L., Schulz, S., & Garbeva, P. (2021). Microbial volatile organic compounds in intra-kingdom and inter-kingdom interactions. *Nature Reviews Microbiology, 19*, 391–404.

Xing, Z., Fu, X., Huang, H., Xu, Y., Wei, L., Shan, C., & Du, Y. (2025). Recent advances in *Lactobacillus plantarum* fermentation in modifying fruit-based products: Flavor property, bioactivity, and practical production applications. *Comprehensive Reviews in Food Science and Food Safety, 24*, Article e70160. https://doi.org/10.1111/1541-4337.70160

Yáñez-Serrano, A. M., Filella, I., LLusià, J., Gargallo-Garriga, A., Granda, V., Bourtsoukidis, E., Williams, J., Seco, R., Cappellin, L., Werner, C., de Gouw, J., & Peñuelas, J. (2021). GLOVOCS - Master compound assignment guide for proton transfer reaction mass spectrometry users. *Atmospheric Environment, 244*, Article 117929. https://doi.org/10.1016/j.atmosenv.2020.117929

Yang, H., Hao, L., Jin, Y., Huang, J., Zhou, R., & Wu, C. (2024). Functional roles and engineering strategies to improve the industrial functionalities of lactic acid bacteria during food fermentation. *Biotechnology Advances, 74*, Article 108397. https://doi.org/10.1016/j.biotechadv.2024.108397

Yang, Z., Al-Dalali, S., Chen, C., Xu, B., Luo, H., & Li, P. (2025). Effect of inoculating *Staphylococcus xylosus* and *Lactiplantibacillus plantarum* on the flavor formation of in-bag dry-aged beef. *International Journal of Food Microbiology, 439*, Article 111237. https://doi.org/10.1016/j.ijfoodmicro.2025.111237

Zhang, X., Zhang, C., Xiao, L., Wang, X., Ma, K., Ji, F., Azarpazhooh, E., Ajami, M., Rui, X., & Li, W. (2024). Gas chromatography-mass spectrometry and non-targeted metabolomics analysis reveals the flavor and nutritional metabolic differences of cow's milk fermented by *Lactiplantibacillus plantarum* with different phenotypic. *Food Bioscience, 60*, Article 104433. https://doi.org/10.1016/j.fbio.2024.104433

Zheng, J., Wittouck, S., Salvetti, E., Franz, C. M. A. P., Harris, H. M. B., Mattarelli, P., O'Toole, P. W., Pot, B., Vandamme, P., Walter, J., Watanabe, K., Wuyts, S., Felis, G. E., Gänzle, M. G., & Lebeer, S. (2020). A taxonomic note on the genus lactobacillus: Description of 23 novel genera, emended description of the genus *Lactobacillus* beijerinck 1901, and union of lactobacillaceae and leuconostocaceae. *International Journal of Systematic and Evolutionary Microbiology, 70*, 2782–2858. https://doi.org/10.1099/ijsem.0.004107

Zwietering, M. H., Jongenburger, I., Rombouts, F. M., & Van 't Riet, K. (1990). Modeling of the bacterial growth curve. *Applied and Environmental Microbiology, 56*, 1875–1881. https://doi.org/10.1128/aem.56.6.1875-1881.1990